ADRC-Driven Trajectory Control of a Quadcopter Considering Ground Effect Dynamics

Carlos Osorio Quero, Jose Martinez-Carranza
Computer Science Department, Instituto Nacional de Astrofisica Optica y Electronica,
Luis Enrique Erro #1, Mexico, Puebla, 72810.

ABSTRACT

The Active Disturbance Rejection Control (ADRC) strategy is designed to mitigate the destabilizing effects of proximity to the ground, commonly known as the ground effect, on quadcopter drones during low-altitude flight. The ground effect introduces complex aerodynamic interactions that compromise flight stability and control precision. The proposed ADRC framework combines feedback linearization with realtime disturbance estimation to address this, enabling robust trajectory tracking despite nonlinear and variable disturbances. High-fidelity Computational Fluid Dynamics (CFD) simulations were used to model ground-effect dynamics and inform controller design. Unlike conventional controllers that rely heavily on computationally intensive CFD models during operation, the ADRC approach adaptively compensates for disturbances, enhancing real-time reliability. The simulation results validate the controller's capacity to maintain accurate altitude and stable flight in ground-effect conditions. These findings highlight the potential of ADRCbased methods to improve the robustness and maneuverability of control in near-ground drone operations.

1 Introduction

Small quadcopter UAVs are increasingly being used for applications such as infrastructure inspection [1], delivery [2], precision agriculture [3], pollution monitoring [4], and search and rescue missions [5]. These tasks often require operation in confined environments and proximity to surfaces, which introduces significant aerodynamic challenges, notably the ground effect (GE) [6].

GE arises from altered airflow patterns near rigid surfaces such as the ground or ceiling, affecting the efficiency of the rotor, reducing the induced velocity, and modifying the aerodynamic drag. Although this effect has been extensively modeled in helicopters and single-rotor systems, multirotor UAVs present greater complexity due to rotor interactions, making accurate GE modeling more difficult.

Although various studies have focused on the characterization of GE, mathematical modeling, and computational fluid dynamics (CFD) simulations [7], most UAV control strategies neglect or avoid GE by maintaining altitude. However, emerging research emphasizes the need for control systems that can actively compensate for these disturbances, especially during low-altitude maneuvers. One such approach is Active Disturbance Rejection Control (ADRC) [8, 9], which offers a model-independent method for the estimation and rejection in real-time of external disturbances such as GE.

In this work, we use CFD simulations (via SolidWorks Flow Simulation) to create high-fidelity aerodynamic data sets under different ground proximities (1 m, 40 cm, 20 cm, 10 cm) with UAVs equipped with 5-inch propellers rotating at 5000–8000 rpm. These data sets validate an ADRC-based trajectory tracking system designed to improve flight stability and accuracy in the presence of strong GE. The proposed framework demonstrates improved performance in scenarios that are critical for UAVs operating in realistic missions near the ground. Therefore, in this work, we propose the following:

- Analyzing the Computational Fluid Dynamics (CFD) of UAVs within and beyond ground effect zones (GE).
- Implementation of ADRC-ESO and RBFNN ADRC-GESO approaches to address perturbations induced by ground effects in UAVs.

2 RELATED WORKS

The study of the effect of ground in rotorcraft has progressed from its origins in helicopter aerodynamics to applications in small UAVs. Early models, such as the one by Cheeseman and Bennett [10] using momentum theory and image methods, laid the foundation by treating the rotor as a point source to predict thrust enhancement and power reduction near the ground. Although widely adopted for UAV control, these quasi-steady models [11], often dependent on normalized rotor height, struggle to generalize between different UAV configurations due to their sensitivity to rotor height, blade geometry, pitch angle, and other design factors.

More recent efforts have expanded to multirotor systems [12] with empirical corrections, yet such models remain limited by singularities near the ground and a dependence on UAV-specific data. To overcome these limitations, researchers are now exploring adaptive, data-driven methods,

^{*}Email address(es): caoq@inaoep.mx

such as machine learning and real-time state estimation, for broader applicability.

Experimental studies using tools such as PIV [13] and force measurements have investigated the behavior of the rotor near partially ground or ceiling surfaces during forward flight, but have not yet produced fast and reliable empirical models. In response, the authors previously introduced an improved quasi-steady model [14] based on the theory of blade elements, which incorporates the pitch, solidity, and rotor geometry of the blade. This model accurately predicts finite IGE thrust [15] and considers dynamic effects such as forward speed and advance ratio, improving thrust estimation and offering practical benefits for UAV control and rotor design, as defined in Eq.(1)[16].

$$\mu = \frac{V_{\infty}}{\|\Omega\| R} \tag{1}$$

 V_{∞} denotes the airspeed in the free stream, which is usually equivalent to the vehicle's true airspeed, and $\|\Omega\|$ represents the rotor's rotational speed. Experimental observations have shown that the advance ratio μ significantly influences the in-ground effect (IGE). However, as Cheeseman and Bennett noted (see Table 1), the thrust enhancement provided by IGE diminishes and can be completely negated when $\mu>0.1$ [17]. In their work [18], they derived an analytical expression for IGE under forward flight conditions, as presented in Eq. (2) [19].

$$K_{IGE} \equiv \frac{T\left(z\right)}{T_{\infty}} = \frac{1}{1 - \frac{1}{16}\left(\frac{R}{Z}\right)^{2} / \left(1 + \left(\frac{V}{v_{i}}\right)^{2}\right)} \quad (2)$$

The interaction between a rotor and the ground, known as the in-ground effect (IGE), significantly alters thrust generation during flight. In this context, V represents the vehicle velocity, while v_i denotes the rotor-induced velocity. The effect of the ground during forward flight has been modeled using a state-space approach [20, 21], predicting a monotonic decrease in the thrust ratio with increasing advance ratio /mu. However, the experimental results [22] reveal nonmonotonic behavior, including a recirculation region for $0.04 \le \mu \le 0.06$ and rotor heights z between 0.6 and 1.2, which reduces rotor thrust. At higher μ values, the ground vortex reintroduces IGE effects. Particle Image Velocimetry (PIV) studies [23] further highlight critical flow characteristics, such as fountain and ground vortices, which correlate with increased power consumption and decreased thrust.

3 ACTIVE DISTURBANCE REJECTION CONTROL WITH A GROUND-EFFECT MODEL

We use an 8-state quadrotor model for translation and rotation, $x\triangleq \begin{bmatrix}z&v_z&\phi&p&\theta&q&\psi&r\end{bmatrix}$ and $u\triangleq \begin{bmatrix}T_{\mathrm{cmd}}&\tau_{\phi}&\tau_{\theta}&\tau_{\psi}\end{bmatrix}$ with known constants g,m, and principal inertias I_x,I_y,I_z . A 12-state ESO (three observer

states per controlled channel $i \in \{z, \phi, \theta, \psi\}$) estimates $[\hat{x}_i, \ \hat{d}_i, \ \hat{d}_i]$, where \hat{d}_i lumps unmodeled dynamics and disturbances. To capture near-ground aerodynamics, the altitude channel introduces a height-dependent thrust multiplier $\gamma(z) \geq 1$ (ground effect). The altitude subsystem of x, $x_z = [z \ v_z]^\top$, evolves as

$$\dot{z} = v_z, \qquad \dot{v}_z = \frac{T_{\rm cmd} \, \gamma(z)}{m} - g,$$
 (3)

Under the small-angle assumption (the inner attitude loop keeps ϕ, θ small, so that the vertical thrust component matches the commanded thrust). The remaining attitude states follow the standard rigid-body rotational dynamics driven by $(\tau_{\phi}, \tau_{\theta}, \tau_{\psi})$. The ESO uses the measured outputs $y = [z \quad \phi \quad \theta \quad \psi]^{\top}$ to update the channel disturbance estimates, with \hat{d}_z absorbing residual model error in (3) and the ground-effect correction through $\gamma(z)$. T_{cmd} is the total thrust commanded by the controller, and $\gamma(z)$ is a ground effect factor that amplifies thrust if the UAV is sufficiently close to the ground. Rotational channels, roll, pitch, and yaw, each follow the basic form of the Euler equations with a rigid body.

3.1 Generalized Extended State Observer (GESO) in the Altitude Loop

We modeled the ground effect with a dimensionless thrust multiplier $\gamma_g(h) \geq 1$, and estimate it online as $\hat{\gamma}_g$ within a generalized extended state observer (GESO). The observer updates $\hat{\gamma}_g$ from the altitude innovation (measured minus predicted). A CFD-derived ground effect map provides $\gamma_g(h)$ via piecewise linear interpolation: it is about 2.2 at $h=0.10\,\mathrm{m}$ and tapers to 1.0 for $h\geq 1\,\mathrm{m}$. Incorporating $\hat{\gamma}_g$ into the vertical control produces height-dependent thrust compensation and improves the low-altitude tracking accuracy. The corrected thrust command is

$$T_{\rm cmd} = \frac{m(g + a_z^{\rm cmd} - \hat{d}_z)}{\operatorname{clip}(\hat{\gamma}_g, 1, \gamma_{\rm max})}, \tag{4}$$

where $\mathrm{clip}(x,1,\gamma_{\mathrm{max}}) = \min\{\max\{x,1\},\gamma_{\mathrm{max}}\}$ ensures physical bounds in the multiplier estimate.

3.2 Control Strategy with Active Disturbance Rejection and Ground-Effect Compensation

Operating multi-rotor UAVs near the ground introduces complex, non-linear aerodynamic disturbances that can destabilize flight. To address this, the proposed control strategy uses radial basis function neural networks (RBFNN) to adaptively tune the gains of the controller. This approach dynamically adjusts the proportional and derivative gains in the roll, pitch and yaw loops based on real-time error states, improving stability and robustness under varying ground-effect conditions Eq. (5).

$$\left(k_{p_{\phi}}, k_{d_{\phi}}, k_{p_{\theta}}, k_{d_{\theta}}, k_{p_{\psi}}, k_{d_{\psi}}\right) = RBFNN\left(e_{\phi}, p, e_{\theta}, q, e_{\psi}, r\right) \tag{5}$$

Table 1: Compares analytical models used to estimate thrust variations under in-ground effect (IGE) conditions. Each model is assessed based on its applicability to multi-rotor platforms and forward flight scenarios, T aerodynamic thrust produced by the rotor system, T_{IGE} thrust generated in ground effect, T_{OGE} thrust generated out of ground effect, T_h OGE hover thrust, T_{out} actual thrust realized in IGE, T_{in} nominal thrust predicted by the OGE, h height of the rotor disk plane AGL [m], R rotor radius, V forward horizontal [m/s], V_h induced velocity in OGE hover [m/s], C_L blade-element lift coefficient.

Model	Multi-rotor	Forward Flight	Ref.
$\frac{T_{IGE}}{T_{OGE}} = \frac{1}{1 - c(h/D)^2} \frac{1}{1 + (H/V)^2}$	No	Yes	Cheeseman [19]
$\frac{T_{IGE}}{T_{OGE}} = \left(0.9926 + 0.03794 \frac{(x/2r)^2}{C_L}\right)^{2/3}$	No	No	Hayden [24]
$ \frac{T_{output}}{T_{input}} = \frac{1}{1 - \rho(\frac{h}{r})^2} $	Yes	No	Danjun [25]
$\frac{T_{IGE}}{T_h} = \frac{1 - \frac{3r}{35}}{1 + \frac{3}{50} \left(\frac{V}{V_h}\right)^3}$	Yes	Yes	Kan [26]

The variables $\{e_\phi, e_\theta, e_\psi\}$ are the attitude errors and $\{p,q,r\}$ are the angular rates. The RBFNN uses a set of Gaussian basis functions that approximate the non-linear mapping from the error space to the controller gains. By training or adaptively tuning these basis functions, the network can:

- Compensation for unmodeled dynamics, such as strong coupling between roll and pitch.
- Respond to changes in operating conditions, including different flight regimes or disturbances.
- Prevent excessive control actions by appropriately distributing or scaling gains.

With these gains based on the neural network, the torque commands for the roll, pitch, and yaw channels become Eq. (6):

$$\tau_{\phi} = \left[\left(k_{p_{\phi}} e_{\phi} + k_{d_{\phi}} \left(\dot{\phi}_{r} - p \right) \right) - \hat{d_{\phi}} \right] b_{0,\phi}
\tau_{\theta} = \left[\left(k_{p_{\theta}} e_{\theta} + k_{d_{\phi}} \left(\dot{\theta}_{r} - q \right) \right) - \hat{d_{\theta}} \right] b_{0,\theta}
\tau_{\psi} = \left[\left(k_{p_{\psi}} e_{\psi} + k_{d_{\psi}} \left(\dot{\psi}_{r} - r \right) \right) - \hat{d_{\psi}} \right] b_{0,\psi}$$
(6)

4 Numerical Validation

This section presents a performance evaluation of the proposed RBFNN-ADRC-GESO controller through four simulation scenarios. Its effectiveness and robustness are evaluated by comparing it with the conventional ADRC-ESO controller under external disturbances and internal model uncertainties. The simulations assume that the quadrotor starts from an initial position and attitude of [0,0,0], with system parameters detailed in Table 2.

Table 2: The parameter values of the quadrotor UAV.

Parameter	Value	Parameter	Value
m (kg)	1.5	I_x (kg/m ²)	0.16
$g (\text{m/s}^2)$	9.8	I_y (kg/m ²)	0.16
l (m)	0.28	I_z (kg/m ²)	0.32

Case 1: The UAV simulation (Fig. 2) evaluates multiaxis control performance over 60 seconds through four distinct flight phases: hovering, climbing with roll, altitude hold with pitch, and descending with yaw. Each phase introduces dynamic

changes in altitude and attitude to test the system's response. Reference signals for altitude and Euler angles are adjusted per phase. The results demonstrate that the ADRC controller, enhanced with a CFD-based ground effect model, ensures accurate tracking across all axes, exhibits fast convergence, minimal overshoot, and robust handling of transient disturbances and model uncertainties near the ground level.

- Case 2: In this test (see Fig. 3(a)), a UAV follows a smooth ascending trajectory with lateral movement while subjected to white noise disturbances $x_d(t) = 6sin(t/3), y_d(t) = -6sin(t/3)cos(t/3)$ and $z_d(t) = 0.8t$. The RBF-ADRC controller shows strong disturbance rejection and precise trajectory tracking, outperforming the standard ADRC controller, which shows oscillations and deviations. The results confirm the effectiveness of integrating RBFNN-based adaptive gain tuning into the ADRC framework.
- Case 3: To assess the robustness of the proposed control framework under model uncertainties (see Fig. 3(b)), a UAV follows a 3D helical trajectory while its physical parameters are reduced by 30% to simulate model mismatch. The RBFNN-ADRC controller, using a GESO-enhanced altitude loop and adaptive gain tuning in the attitude channel, maintains accurate tracking despite uncertainties. In contrast, the standard ADRC shows increased error. The results confirm that the RBFNN-ADRC structure enhances robustness and performance under dynamic and uncertain conditions. The reference path is defined as $x_d(t) = R\cos(\omega t)$, $y_d(t) = R\sin(\omega t)$ and $z_d(t) = z_0 + ct$, where R = 20 m, $\omega = 0.2$ rad/s, c = 1 and $z_0 = 10$ m.
- Case 4: The target trajectory begins with a vertical ascent for the first 5 seconds (see Fig. 3(c)), followed by a circular path in the horizontal plane at a constant altitude. System robustness is tested by applying a Gaussian-shaped wind disturbance along the z-axis, Eq 7.

$$a_{wind,y}(t) = A \cdot exp\left(-\frac{1}{2}\left(\frac{t-t_0}{\sigma_t}\right)^2\right)$$
 (7)

4.1 RBFNN-ADRC Control of UAVs in Ground Effect: Discussion

The proposed RBFNN-ADRC control strategy significantly improves the performance of the UAV in ground-effect scenarios compared to traditional ADRC. Evaluated across three flight scenarios

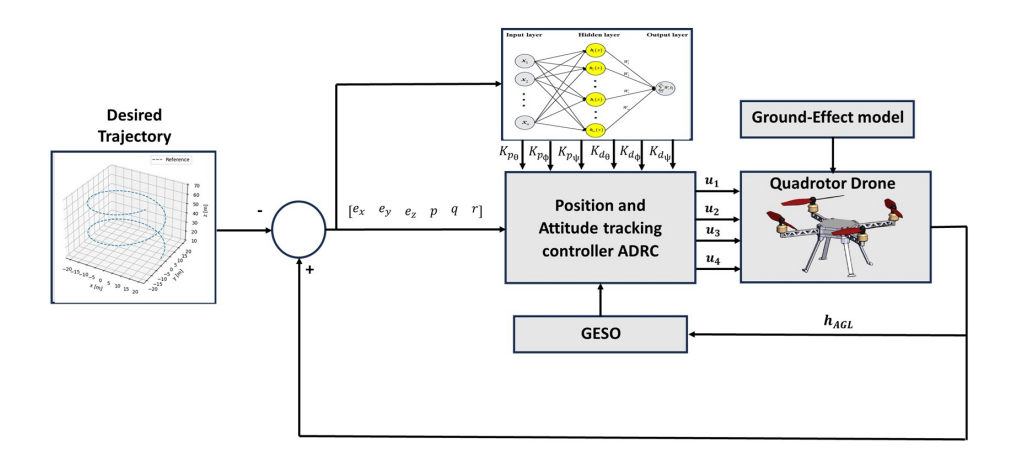


Figure 1: The diagram illustrates the control framework combining a GESO with an ADRC augmented by an RBFNN. The system tracks a predefined 3D trajectory by computing tracking errors $\begin{bmatrix} e_x & e_y & e_z & p & q & r \end{bmatrix}$, which the RBFNN processes to tune attitude control adaptively gains $(k_{p_\theta}, k_{d_\theta}, k_{p_\phi}, k_{d_\phi}, k_{p_\psi}, k_{d_\phi})$. These gains are fed into the ADRC to generate control inputs (u_1, u_2, u_3, u_4) for the quadrotor drone. The GESO block estimates altitude states, measured altitude above ground (AGL) from the downward range sensor h_{AGL} and compensates for ground effect disturbances in real time, enhancing the controller's robustness near surfaces. The closed-loop feedback integrates drone dynamics, ground effect modeling, and adaptive gain scheduling to ensure stable and accurate flight performance.

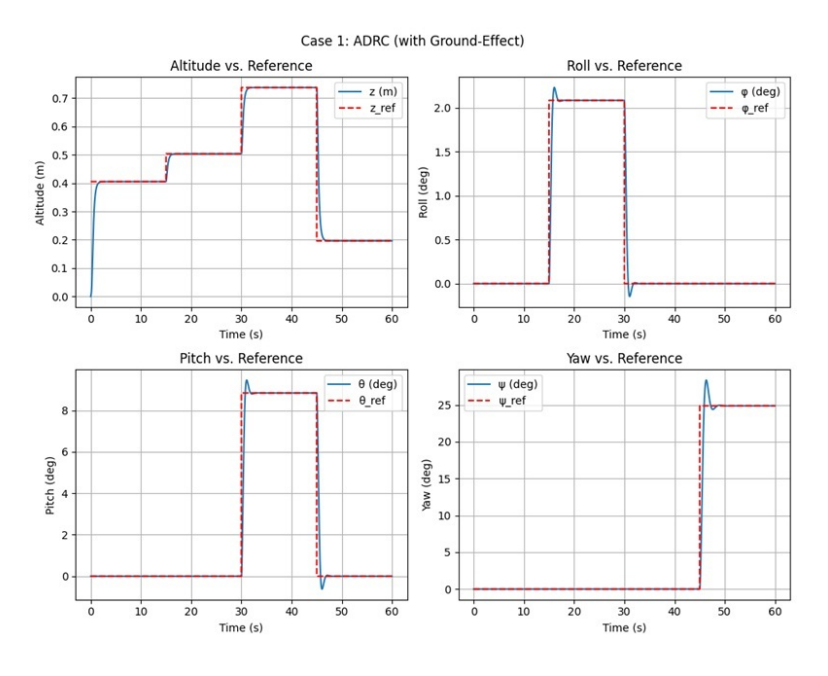


Figure 2: In this scenario, the UAV follows a phase-based reference trajectory over a 60-second simulation, divided into four distinct operational phases: hovering, ascending, pitching/rolling maneuvers, and descending with yaw rotation.

using error metrics (ISE, ITSE, IAE, ITAE), RBFNN-ADRC consistently shows superior tracking accuracy and robustness, particularly under dynamic disturbances. For example, in Scenario 1, the ISE is compared to ADRC, and in Scenario 3, it achieves a much lower ITAE despite external perturbations. Further analysis of ground-effect models within the RBFNN-ADRC framework reveals that the Dnajun model yields the best control accuracy. These findings highlight the benefit of integrating adaptive neural controllers with accu-

rate physical models to enhance UAV stability in low-altitude environments.

5 CONCLUSION

This work introduces a robust control strategy that combines ADRC with GESO and RBFNN tuning to effectively counteract ground-effect disturbances in UAVs. A key innovation is the integration of a CFD-based empirical model for ground effect, allow-

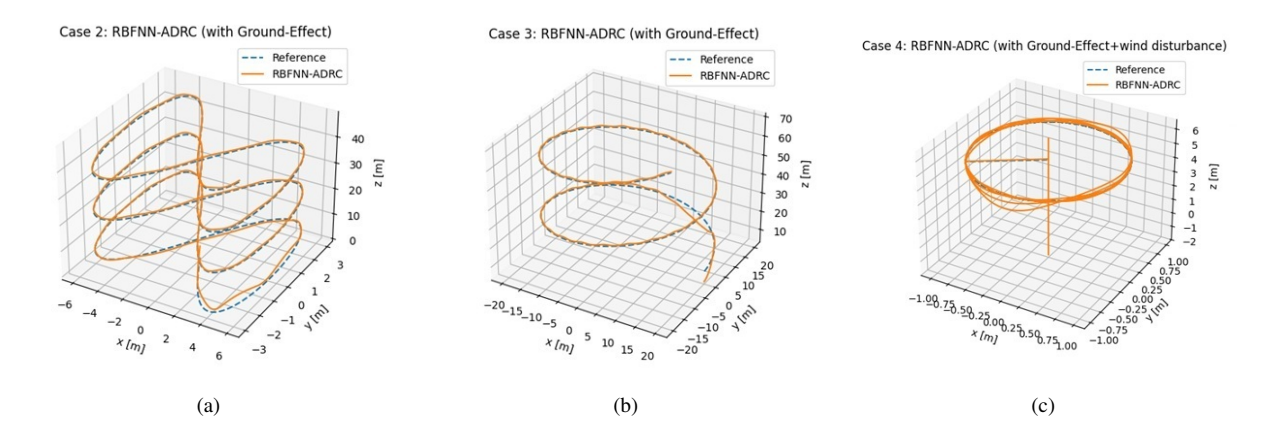


Figure 3: Trajectory Tracking and Disturbance Rejection Using RBFNN-ADRC with Ground Effect: (a) Case 2 $x_d(t) = 6sin(t/3), y_d(t) = -6sin(t/3)\cos(t/3)$ and $z_d(t) = 0.8t$, incorporating lateral motion, (b) Case 3- controller configurations are preserved, while the altitude loop is enhanced using a Generalized Extended State Observer (GESO) informed by a CFD-based, data-driven ground-effect model, (c) Case 4- controller configurations are preserved, with the altitude control loop enhanced via a Generalized Extended State Observer (GESO), which incorporates a CFD-informed, data-driven ground-effect model to improve compensation near the ground. In addition, a lateral wind disturbance is introduced along the y axis to simulate real-world aerodynamic perturbations that affect the stability of the quadrotor.

Table 3: Evaluation of the Control Performance of the Proposed ADRC Strategy with ESO and RBFNN-Augmented GESO for Mitigating Ground Effect Disturbances.

Controller	ISE	ITSE	IAE	ITAE
$PID_{Scenario\ 1}$	XX	XX	XX	XX
$PID_{Scenario\ 2}$	xx	XX	xx	xx
$PID_{Scenario\ 3}$	XX	XX	xx	xx
$ADRC_{Scenario\ 1}$	3.26	38.25	5.23	153.25
$ADRC_{Scenario\ 2}$	2.42	35.75	5.02	167.84
$ADRC_{Scenario\ 3}$	2.57	37.24	5.84	176
$RBFNN - ADRC_{Scenario\ 1}$	1.64	14.5	1.4	80.8
$RBFNN - ADRC_{Scenario\ 2}$	1.92	23.1	2.82	70
$RBFNN - ADRC_{Scenario\ 3}$	1.2	25.6	2.93	72.5
$RBFNN - ADRC_{Scenario\ 4}$	1.34	34.6	2.83	82.5

Table 4: Performance index Ground-Effect models for RBFNN-ADRC model proposed.

Models	ISE	ITSE	IAE	ITAE
Dnajun	1.2	29.73	2.56	71.90
Hayden	1.53	28.65	2.42	71.50
Cheeseman	1.58	21.06	2.38	74.43
Kan	1.42	24.06	2.86	85.56

ing accurate lift compensation during low-altitude flight. Embedded within the control loop, this model improves precision by capturing real aerodynamic interactions. Simulations in ROS demonstrate that the proposed RBFNN-ADRC outperforms standard ADRC across all error metrics, with ITAE in one scenario nearly halved. The Dnajun model was found to offer the best balance between accuracy and stability. Overall, the approach enables scalable, real-time control for UAV missions near the ground, such as terrain following and

autonomous landing.

ACKNOWLEDGEMENTS

The first author is thankful to the National Council for Technological and Scientific Research (CONACYT) No. CVU: 661331.

REFERENCES

- [1] Ioannis Pitas. Drone vision and deep learning for infrastructure inspection. In 2021 IEEE International Conference on Autonomous Systems (ICAS), pages 1–1, 2021.
- [2] Suttinee Sawadsitang, Dusit Niyato, Puay-Siew Tan, and Ping Wang. Joint ground and aerial package delivery services: A stochastic optimization approach. *IEEE Transactions on Intelligent Transportation Systems*, 20(6):2241–2254, 2019.
- [3] Songchao Zhang, Xinyu Xue, Chen Chen, Zhu Sun, and Tao Sun. Development of a low-cost quadrotor uav based on adrc for agricultural remote sensing. *International Journal of Agricultural and Biological Engineering*, 12(4):82–87, 2019.

- [4] Ranganathan Rani Hemamalini, Rajasekaran Vinodhini, Balusamy Shanthini, Pachaivannan Partheeban, Mani Charumathy, and Karunakaran Cornelius. Air quality monitoring and forecasting using smart drones and recurrent neural network for sustainable development in chennai city. Sustainable Cities and Society, 85:104077, 2022.
- [5] Carlos Osorio Quero and Jose Martinez-Carranza. Unmanned aerial systems in search and rescue: A global perspective on current challenges and future applications. *International Jour*nal of Disaster Risk Reduction, 118:105199, 2025.
- [6] C. Paz, E. Suárez, C. Gil, and C. Baker. Cfd analysis of the aerodynamic effects on the stability of the flight of a quadcopter uav in the proximity of walls and ground. *Journal of Wind Engineering and Industrial Aerodynamics*, 206:104378, 2020
- [7] Sam Dougherty, Nay Lin Oo, and Dan Zhao. Effects of propeller separation and onset flow condition on the performance of quadcopter propellers. *Aerospace Science and Technology*, 145:108837, 2024.
- [8] Mario Ramírez-Neria, Alberto Luviano-Juárez, Jaime González-Sierra, Rodrigo Ramírez-Juárez, Joaquín Aguerrebere, and Eduardo G. Hernandez-Martinez. Active disturbance rejection control for the trajectory tracking of a quadrotor. *Actuators*, 13(9), 2024.
- [9] Sofiane Khadraoui, Raouf Fareh, Mohammed Baziyad, Mahmoud Bakr Elbeltagy, and Maamar Bettayeb. A comprehensive review and applications of active disturbance rejection control for unmanned aerial vehicles. *IEEE Access*, 12:185851–185868, 2024.
- [10] Chin Gian Hooi, Francis D. Lagor, and Derek A. Paley. Flow sensing, estimation and control for rotorcraft in ground effect. In 2015 IEEE Aerospace Conference, pages 1–8, 2015.
- [11] Xiang He, Gordon Kou, Marc Calaf, and Kam K. Leang. In-ground-effect modeling and nonlinear-disturbance observer for multirotor unmanned aerial vehicle control. *Journal of Dy*namic Systems, Measurement, and Control, 141(7):071013, 05 2019.
- [12] H. Nobahari and A.R. Sharifi. Continuous ant colony filter applied to online estimation and compensation of ground effect in automatic landing of quadrotor. *Engineering Applications of Artificial Intelligence*, 32:100–111, 2014.
- [13] Iain Fairley, Benjamin J. Williamson, Jason McIlvenny, Nicholas King, Ian Masters, Matthew Lewis, Simon Neill, David Glasby, Daniel Coles, Ben Powell, Keith Naylor, Max Robinson, and Dominic E. Reeve. Drone-based large-scale particle image velocimetry applied to tidal stream energy resource assessment. *Renewable Energy*, 196:839–855, 2022.
- [14] Charbel Hage, Tonino Sophy, and El Hassane Aglzim. A comprehensive study on the aerodynamic influence of stationary and moving obstacles on an isolated phantom dji 3 uav propeller. *The Journal of Engineering*, 2024(4):e12374, 2024.
- [15] Jielong Cai and Sidaard Gunasekaran. Propeller ceiling effect in forward flight. *Journal of Aircraft*, 61(4):1230–1246, 2024.
- [16] Xiang He and Kam K. Leang. Quasi-steady in-ground-effect model for single and multirotor aerial vehicles. *AIAA Journal*, 58(12):5318–5331, 2020.

- [17] Ambar Garofano-Soldado, Antonio Gonzalez-Morgado, Guillermo Heredia, and Anibal Ollero. Assessment and modeling of the aerodynamic ground effect of a fully-actuated hexarotor with tilted propellers. *IEEE Robotics and Automation Letters*, 9(2):1907–1914, 2024.
- [18] Ke Yu and David A Peters. Nonlinear three-dimensional statespace modeling of ground effect with a dynamic flow field. *Journal of the American Helicopter Society*, 50(3):259–268, 2005.
- [19] Chin Gian Hooi, Francis D. Lagor, and Derek A. Paley. Flow sensing, estimation and control for rotorcraft in ground effect. In 2015 IEEE Aerospace Conference, pages 1–8, 2015.
- [20] P-M Basset, O Heuze, JVR Prasad, and M Hamers. Finite state rotor induced flow model for interferences and ground effect. In AHS-International Forum 57, 2001.
- [21] Pedro Sanchez-Cuevas, Guillermo Heredia, and Anibal Ollero. Characterization of the aerodynamic ground effect and its influence in multirotor control. *International Journal of Aerospace Engineering*, 2017(1):1823056, 2017.
- [22] Zhenlong WU, Tianyu ZHANG, Huijun TAN, Haoyu ZHOU, Wei CHEN, and Maixiang XIE. Hovering rotor aerodynamics in extreme ground effect. *Chinese Journal of Aeronautics*, 37(7):204–219, 2024.
- [23] Jielong Cai, Sidaard Gunasekaran, and Michael Ol. Effect of partial ground and partial ceiling on propeller performance. *Journal of Aircraft*, 60(3):648–661, 2023.
- [24] Lokesh Silwal, Mahendra Bhagwat, and Vrishank Raghav. Aerodynamic interactions of counter-rotating coaxial rotors hovering in ground effect. *Journal of Aircraft*, 59(6):1416– 1425, 2022.
- [25] Li Danjun, Zhou Yan, Shi Zongying, and Lu Geng. Autonomous landing of quadrotor based on ground effect modelling. In 2015 34th Chinese Control Conference (CCC), pages 5647–5652, 2015.
- [26] Xinyue Kan, Justin Thomas, Hanzhe Teng, Herbert G. Tanner, Vijay Kumar, and Konstantinos Karydis. Analysis of ground effect for small-scale uavs in forward flight. *IEEE Robotics* and Automation Letters, 4(4):3860–3867, 2019.
- [27] Nay Lin Oo, Dan Zhao, Mathieu Sellier, and Xiran Liu. Experimental investigation on turbulence effects on unsteady aero-dynamics performances of two horizontally placed small-size uav rotors. Aerospace Science and Technology, 141:108535, 2023.
- [28] Francisco M. F. R. Gonçalves, Ryan M. Bena, and Néstor O. Pérez-Arancibia. Closed-loop stability of a lyapunov-based switching attitude controller for energy-efficient torque-input-selection during flight. In 2024 IEEE International Conference on Robotics and Biomimetics (ROBIO), pages 1941–1947, 2024.
- [29] Liguo Zhang, Ying Lu, Yangzhou Chen, and Nikos E. Mastorakis. Robust uniformly ultimate boundedness control for uncertain switched linear systems. *Computers Mathematics with Applications*, 56(7):1709–1714, 2008.

APPENDIX A: THE QUADROTOR MODEL UNDER THE GROUND EFFECT

This study investigates the aerodynamic behavior of a quadrotor drone that flows into and out of the ground effect (IGE / OGE) using SolidWorks flow simulation. With equalized thrust at a fixed rotor speed of 8000 rpm (through pitch control), the simulation shows a thrust peak at a height-to-diameter ratio (h/D) of 0.5. Various aerodynamic models, particularly Danjun and Kan, are evaluated for their suitability to model multirotor IGE dynamics [27], although they often oversimplify near-ground airflow. The simulated drone features 5-inch propellers and an L/R ratio of 2.8, with a computational domain carefully dimensioned to minimize boundary effects (see Fig. 4). Simulations solve the RANS equations using the SST turbulence model, combining k– ω and k– ϵ methods based on proximity to the ground, with numerical settings optimized for accuracy and stability (see Fig. 5).

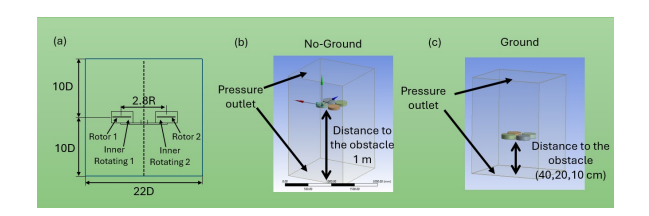


Figure 4: Simulation settings used in this study: Schematic representation, (a) quadcopter setup, (b) no-ground condition, and (c) ground condition

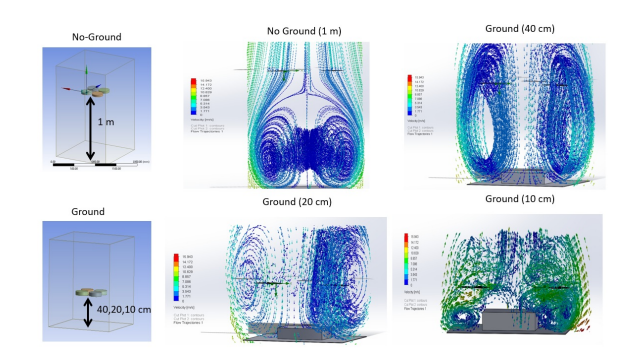


Figure 5: Simulation on Solidworks flow simulation settings study case no-ground (1 m) and ground proximity scenarios (40 cm, 20 cm, 10 cm) scenarios, operating at high rotational speeds of 8000 rpm.

APPENDIX B: GROUND EFFECT MODELING USING CFD-ADJUSTED EMPIRICAL MODELS

An empirical model based on CFD simulation data was developed to account for the ground effect during low-altitude drone flight. The model introduces a correction factor, M(z), which varies with the height of the rotor: it is interpolated for altitudes below 1.0 m and set to 1 above that threshold, where the ground effect is negligible. This approach improves simulation accuracy and supports the design of more reliable control algorithms for near-ground

operations.

$$M\left(z\right) = \begin{cases} 1 & z \ge 1m \\ \min\left(\frac{1}{1 - \left(\frac{r}{4z}\right)^2}, 1.3 - 0.5\left(z - 0.4\right)\right) & 0.4 \le z < 1m \\ \min\left(\frac{1}{1 - \left(\frac{r}{4z}\right)^2}, 1.6 - 1.5\left(z - 0.2\right)\right) & 0.2 \le z < 0.4m \\ \min\left(\frac{1}{1 - \left(\frac{r}{4z}\right)^2}, 2.2 - 6\left(z - 0.1\right)\right) & 0.1 \le z < 0.2m \\ 2.2 & z < 0.1m \\ (8) \end{cases}$$

- Cheeseman model with CFD correction: $\hat{GE}_{CFD} = \hat{GE}_{Cheeseman}xM\left(z\right)$
- Hayden model with CFD correction:

$$\hat{GE}_{Hayden} = \begin{cases} \left(0.9926 + 0.03794 \frac{(z/2r)^2}{C_L}\right)^{2/3} & 0.1 \le z < 1m \\ 2.2 & z < 0.1m \\ 1 & z \ge 1m \end{cases}$$

where r is the rotor radius and C_L is the lift coefficient.

- Kan model with CFD correction: $\hat{GE}_{kan} = \left(1 \frac{3r}{35}\right) / \left(1 + \frac{3}{50} \left(\frac{V}{V_h}\right)^3\right) xM\left(z\right)$ where V is the actual climb velocity and V_h is the hovering-induced velocity.
- Dnajun model with CFD correction: $\hat{GE}_{CFD} = \hat{GE}_{Dnajun}xM(z)$

APPENDIX C: STABILITY ANALYSIS VIA LYAPUNOV THEORY

A Lyapunov-based stability analysis is performed for the altitude control subsystem [28] to evaluate the robustness of the proposed RBFNN-ADRC-GESO control strategy against wind-induced disturbances and near-ground aerodynamic effects. Let the altitude tracking error be defined as $e_z = z(t) - z_r(t)$ and $e_{\dot{z}} = \dot{z}(t) - \dot{z}_r(t)$, where $\dot{z}(t)$ is the desired altitude trajectory and $\dot{z}_r(t)$ it is a time derivative. A candidate Lyapunov function is proposed as Eq. (10):

$$V(t) = \frac{1}{2}e_z^2(t) + \frac{1}{2}e_{\dot{z}}^2(t)$$
 (10)

This positive definite function measures the total instantaneous tracking energy in the altitude channel. Taking its time derivative yields the following Eq. (11).

$$\dot{V}(t) = e_z(t) \cdot \dot{e}_z(t) + e_{\dot{z}}(t) \cdot \dot{e}_{\dot{z}}(t) \tag{11}$$

Substituting the tracking error dynamics governed by closed-loop altitude dynamics, and incorporating the observer-based disturbance estimation \hat{f}_{ext} , we obtain Eq. (12).

$$\dot{e}_z = e_{\dot{z}}, \quad \dot{e}_{\dot{z}} = \frac{1}{m} T_z - g - \ddot{z}_r \left(t \right) + \Delta \left(z, \dot{z}, t \right), \quad (12)$$

where Δ (.) includes the lumped uncertainty from ground-effect correction $M_{GE}(z)$ and wind-induced perturbations. The control input T_z is designed as Eq. (13):

$$T_z = m \cdot \left(\ddot{z}_r(t) - k_p e_z - k_d e_{\dot{z}} + \hat{f}_{ext} \right)$$
 (13)

Substituting Eq. (12) into Eq. (11):

$$\dot{V}(t) = -k_p e_z^2 - k_d e_{\dot{z}}^2 + e_{\dot{z}} \cdot \left(\Delta - \hat{f}_{ext}\right) \tag{14}$$

Assume a bounded disturbance estimation error $\left|\Delta - \hat{f}_{ext}\right| \leq \varepsilon$, and applying Young's inequality Eq. (15) and Eq. (16).

$$e_{\dot{z}} \cdot \left(\Delta - \hat{f}_{ext}\right) \le \frac{1}{2} k_d e_{\dot{z}}^2 + \frac{\varepsilon^2}{2k_d}$$
 (15)

$$\dot{V}(t) \le -k_p e_z^2 - \frac{1}{2} k_d e_z^2 + \frac{\varepsilon^2}{2k_d}$$
 (16)

APPENDIX D: LYAPUNOV STABILITY RBFNN ADAPTATION

The attitude control gains k_{pi}, k_{di} for $i \in \{\phi, \theta, \psi\}$ are adaptively generated using a Radial Basis Function Neural Network (RBFNN) Eq. (17):

$$\begin{bmatrix} k_{pi}(t) & k_{di}(t) \end{bmatrix} = \sum_{j=1}^{N} \omega_{ij} \phi_{j}(e(t))$$
 (17)

where $\phi\left(\cdot\right)$ are Gaussian basis functions on the state error vector $e=\left[e_{i},\omega_{i}\right]^{T}$, where the basis functions are normalized $\sum_{j}\phi_{j}\left(\cdot\right)\leq1$, ω_{ij} are trained weights bounded $\omega_{ij}\in\left[\omega_{min},\omega_{max}\right]$. Hence, the adaptive gains are positive and bounded $0< k_{pi}^{min}\leq k_{pi}\left(t\right)\leq k_{pi}^{max}, 0< k_{di}^{min}\leq k_{di}\left(t\right)\leq k_{di}^{max}$. Let us define a Lyapunov function for each attitude channel $V_{i}\left(t\right)=\frac{1}{2}e_{i}^{2}+\frac{1}{2}\omega_{i}^{2}$, using a similar derivation $\dot{V}_{i}\leq\left(t\right)-\lambda_{1}\left\|e_{i}\right\|^{2}-\lambda_{2}\left\|\omega_{i}\right\|^{2}+\delta_{i}\left(t\right)$, where $\lambda_{1},\lambda_{2}>0$ depend on the adaptive gain bounds, and δ_{i} is a bounded disturbance term from the modeling error or external wind. As a result, the attitude subsystem is guaranteed to eventually be uniformly bounded (UUB) [29] under the adaptive control strategy based on the RBFNN.